Synthesis and Reactivity of Ampy-based Ruthenium(II) Catalysts for Transfer Hydrogenation of Ketones

Edith K. Amason^a, Khashayar Rajabimoghadam^c, Notashia N. Baughman^b, C. Roland Ghareeb^a,

Samantha K. Bourgeois^a, Channita Keuk^a, Gayle Manacsa^a, Brian V. Popp^b, Isaac Garcia
Bosch^e, Gregory M. Ferrence^d and Evan E. Joslin^{a,*}

Department of Chemistry, The University of the South, Sewanee, TN 22903, USA; ^bC. Eugene Bennett Department of Chemistry, West Virginia University, Morgantown, West Virginia,
26505, USA; ^cDepartment of Chemistry, Southern Methodist University, Dallas, TX, 75275,
USA; ^dDepartment of Chemistry, Illinois State University, Normal, IL 61790, USA; ^eDepartment of Chemistry, Carnegie Mellon University, Pittsburg, PA 15213, USA.

*eejoslin@sewanee.edu

Abstract: Four ruthenium(II) complexes of the motif, *cis*-RuCl₂[Ph₂P(CH₂)₄PPh₂](ampy-L) and *trans*-RuCl₂[Ph₂P(CH₂)₄PPh₂](ampy-L) (ampy = 2-(aminomethyl)pyridine; L = Cl or OMe) were synthesized for potential catalytic applications. The complexes were fully characterized using NMR spectroscopy, UV-Vis spectroscopy, X-ray crystallography and electrochemical analysis. The *trans* isomer was observed to undergo isomerization to the *cis* isomer, and kinetic studies of the isomerization reaction showed that the subtle changes in ampy-L electron density did not impact the rate of *trans-to-cis* isomerization. To probe these complexes' utility towards catalysis, transfer hydrogenation for the reduction of a variety of ketones were performed. All three complexes showed high rates and yields towards ketone transfer hydrogenation.

Introduction

The reactivity of a large array of ruthenium(II) complexes, with differing electronic and steric profiles, have been explored in detail. ^{1–6} Previous studies have shown that varying the electronics of a metal center and the associated ligands often has a significant impact on catalytic activity. ⁷ A common method for changing the electron density of a metal center is to vary the phosphine ligand. Phosphine ligands are often altered due to the large electronic and steric profiles that these versatile ligands provide. ^{8,9} Another ligand that has allowed for a wide range of electronic modification while limiting steric changes around the metal center, is the 4,4'-substituted bipyridine ligand. Alternatively, our group is interested in studying the electronic effects embedded in the use of an aminopyridine ligand rather than bipyridine. We hypothesize that alteration of the aminopyridine ligand will cause more subtle changes in electron density given only one group in the *para*-position is being changed. This subtle change could potentially allow for a finer tunability in catalysis reactions.

Current research has shown that ruthenium(II) complexes containing 2-(aminomethyl)pyridine (ampy) ligands are capable of dehydrogenation, isomerization, racemization, and deuteration reactions. ^{10,11} Specifically, significant work has been dedicated to the study of ruthenium(II) complexes containing both phosphine and N-donor ligands and their catalytic activity towards hydrogenation reactions. ^{11–16} These complexes are utilized for the production of ketones, lactones, imines, epoxides, carboxylic acids, and other reducible bonds. ¹⁷

The ability to selectively transfer a functional group on a molecule while leaving other functional groups intact is a critical modification utilized in both the pharmaceutical and synthetic industries.^{18–20} One example of such a transformation is the catalytic transfer of hydrogen.^{21–23} Since the pioneering work of Noyori and co-workers, the use of ruthenium-diamine catalysts for transfer hydrogenation has continued to grow.^{24–27} The Baratta group continued to examine catalytic transfer hydrogenation reactions utilizing isolatable ruthenium(II) complexes with the 2-(aminomethyl)pyridine, ampy, ligand. Specifically, they examined the effect of a variety of phosphine ligands on catalysis; however, did not examine the effects of substituting the ampy ligand.¹⁰

Herein we report the synthesis of multiple ruthenium diphosphine-aminopyridine complexes with the replacement of the *para*-hydrogen on the pyridine ring with a more electron donating group or an electron withdrawing group. These complexes have been characterized through NMR spectroscopy, UV-Vis, X-ray crystallography, and cyclic voltammetry to determine the effect of these groups on the electron density of the ruthenium metal center. Additionally, catalytic transfer hydrogenation experiments and *trans-to-cis* isomerization reactions were conducted to gain a fuller understanding of reactivity.

Results and Discussion

A. Synthesis and characterization of cis-RuCl₂(dppb)(ampy-L)

complexes cis-RuCl₂[Ph₂P(CH₂)₄PPh₂](ampy-Cl) (ampy-Cl = 4-chloro-2aminomethylpyridine (1) and cis-RuCl₂[Ph₂P(CH₂)₄PPh₂](ampy-OMe) (ampy-OMe = 4-methoxy-2-aminomethylpyridine) similar **(2)** were synthesized manner cis-RuCl₂[Ph₂P(CH₂)₄PPh₂](ampy) (3) (Scheme 1, Top). ¹⁰ This synthetic procedure requires the prior isolation of RuCl₂(dppb)PPh₃ (dppb = Ph₂P(CH₂)₄PPh₂) a complex which reacted in toluene with a slight excess of ampy-Cl or ampy-OMe under reflux for 20 hours. The complexes precipitate out of solution; hence they are easily collected via vacuum filtration in moderately high yields of pure material. An alternative single pot synthetic procedure can also yield pure complex in similar yields (Scheme 1, Bottom). 10 A mixture of RuCl₂(PPh₃)₃ and ampy-Cl or ampy-OMe were stirred in toluene for one hour to yield a homogenous solution. Then 1,4-bis(diphenylphosphino)butane (dppb) was added to the solution and refluxed overnight. The resulting bright yellow precipitate was again easily isolated as the pure complex in a moderate yield. Notably, concentration of the reaction solution or inducing precipitation to increase the final yield, as in the published report for complex 3, yielded unwanted impurities that could not be removed from the final product.¹⁰

$$\begin{array}{c} Ph_2 \\ Ph_2 \\ Ph_3 \\ Ph_2 \\ Ph_3 \\ Ph_2 \\ Ph_3 \\ Ph_2 \\ Ph_3 \\ Ph_2 \\ Ph_3 \\ Ph_4 \\ Ph_3 \\ Ph_3 \\ Ph_3 \\ Ph_3 \\ Ph_4 \\ Ph_5 \\ Ph$$

Scheme 1. Synthetic Pathways for *cis*-RuCl₂(dppb)(ampy-L).

Unlike the more commonly studied Ru(dppb)(bipyridine) complexes, bidentate coordination of the ampy ligand can lead to three possible isomers. When using the aminopyridine ligand, the overall cis orientation of the complex can generate two alternate coordination orientations for the aminopyridine ligand in addition to the single trans-orientation. In the orientation referred to as *cis*-isomer 1, the pyridine is *trans* to the phosphine while the amine is trans to the chloride. If the aminopyridine ligand is reversed, another isomer, cis-isomer 2 is generated (Figure 1). To verify the configuration of the synthesized complexes, suitable single Xray quality crystals for complexes 1 and 2 (Figure 2 and Figure 3) were obtained by diffusion of pentane into a chloroform solution of the complex. Crystallographic data confirmed the orientation of the ampy ligand in both complexes was cis-isomer 1, where the pyridine is trans to the phosphine and the amine is *trans* to the chloride. Comparison of the structures of complexes 1 and 2 with the previously reported structure for complex 3 shows minimal changes in bond lengths and angles. 10 As previously seen, the Ru-Cl bond length *trans* to the nitrogen is slightly shorter than the Ru-Cl bond length trans to the phosphorus. Additionally, a similar trend is observed for the N1-Ru-N2, C11-Ru-N1 and C12-Ru-N1 angles (Table 1, Table 2), confirming a distorted octahedral geometry around the metal centers.

Figure 1. Possible isomers for RuCl₂(dppb)(ampy-L).

Table 1. Selected Crystallographic Data for *cis*-RuCl₂(dppb)(ampy-Cl) (1), *cis*-RuCl₂(dppb)(ampy-OMe) (2), and *cis*-RuCl₂(dppb)(ampy)(3). ¹⁰

	complex 1•(CHCl ₃)	complex 2•(CHCl ₃) _{1.5}
empirical formula	$C_{35}H_{34}Cl_6N_2P_2Ru$	$C_{36.5}H_{39.5}Cl_{6.5}N_2OP_2Ru$
fw	858.35	915.65
Temp (K)	173(2)	173(2)
cryst syst	monoclinic	monoclinic
space group	$P2_1/n$	$P2_1/c$
a, Å	21.8459(11)	14.4629(6)
b, Å	14.3541(7)	25.6963(9)
c, Å	24.0168(12)	11.2643(4)
β, deg	105.889(3)	111.515(2)
$V, A^{\bar{3}}$	7243.4(6)	3894.4(3)
Z	8	4
D _{calcd} , mg/m ³	1.578	1.562
Absorption Coefficient	0.993 mm ⁻¹	0.964 mm ⁻¹
cryst size (mm)	0.170 x 0.238 x 0.422	0.32 x 0.13 x 0.06
R1, wR2 $(I > 2(I))$	0.0313, 0.0683	0.0321, 0.0612
GOF	1.082	1.037

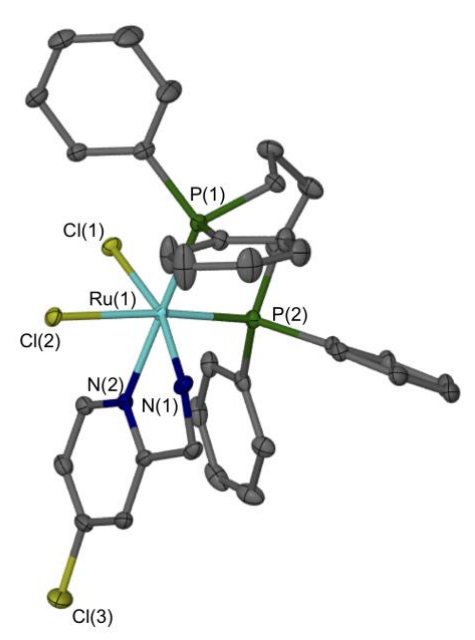


Figure 2. Crystal structure of *cis*-RuCl₂(dppb)(ampy-Cl)•CHCl₃ (1) (50% probability with hydrogen atoms omitted for clarity).

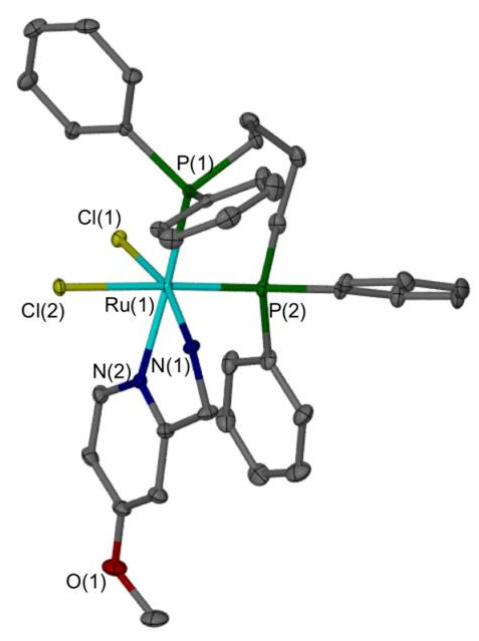


Figure 3. Crystal structure of *cis*-RuCl₂(dppb)(ampy-OMe)•1.5CHCl₃ (2) (50% probability with hydrogen atoms omitted for clarity).

Table 2. Comparison of bond lengths (Å) and Angles (°) for 1•CHCl₃, 2•1.5CHCl₃ and 3.¹⁰

	ampy-Cl (1)	ampy-OMe (2)	ampy (3)
Ru-N1	2.1234(15)	2.1040(16)	2.116(2)
Ru-N2	2.1287(14)	2.1494(16)	2.148(2)
Ru-P1	2.2855(5)	2.2786(5)	2.2874(6)
Ru-P2	2.2841(4)	2.2756(5)	2.2825(6)
Ru-Cl1	2.4179(4)	2.4530(5)	2.4415(5)
Ru-C12	2.4944(4)	2.4768(5)	2.4899(5)
Cl1-Ru-Cl2	90.719(15)	90.115(16)	89.75(2)
P1-Ru1-Cl2	93.748(16)	88.899(17)	93.45(2)
P2-Ru1-Cl2	172.157(16)	176.367(18)	173.36(2)
N1-Ru1-Cl2	79.63(4)	82.92(5)	81.22(6)
N2-Ru1-Cl2	83.02(4)	84.20(4)	82.78(5)
P1-Ru1-Cl1	93.580(16)	97.537(17)	94.98(2)
P2-Ru-Cl1	87.081(16)	87.556(17)	87.81(2)
N1-Ru-Cl1	166.20(4)	164.89(4)	166.23(6)
N2-RuCl1	91.66(4)	89.45(4)	91.65(5)
P1-Ru-P2	93.903(16)	94.169(18)	92.92(2)
P1-Ru-N1	96.85(4)	95.73(4)	95.92(5)
P1-Ru-N2	173.88(4)	170.20(4)	172.36(5)
P2-Ru-N1	96.85(4)	95.73(4)	100.00(6)
P2-RuN2	89.52(4)	92.99(4)	91.11(5)
N1-Ru-N2	77.49(6)	76.55(6)	76.98(7)

Density functional theory studies of complexes **1-3** were initiated to complement experimental analyses. DFT functional benchmarking studies comparing experimental metrical data to that calculated for parent complex **3** revealed geometry optimization with PBE0 and BP86 using LANL2TZ(f)/LANL2 for ruthenium and 6-31+G(d) for all other atoms best reproduced experimental values while functional M06 systematically overestimated bond lengths (Table S3). Metrical comparison of DFT optimized complexes **1-3** shows similar trends with *para* substitution to the ampy ligand as observed in the X-ray diffraction data above (Table S3).

Complexes 1 and 2 were characterized by ¹H, ¹³C{¹H}, and ³¹P{¹H} NMR spectroscopy. The NMR spectra of complexes 1 and 2 are similar to the previously reported cis-RuCl₂(dppb)(ampy) with a few distinguishing differences. The ¹H NMR spectra show a total of 23 hydrogens in the aromatic region which is consistent with the replacement of a proton with a chloride or a methoxy group at the para-position of the pyridine ring. The biggest shifts in the NMR spectra are for the protons located on the pyridine ring, specifically the *meta*-protons (with respect to the nitrogen). Complex 2 displays two upfield resonances at 6.24 ppm and 6.33 ppm; whereas, only one resonance is observed for complexes 1 and 3 at 6.75 ppm and 6.73 ppm, respectively. The other *meta*-proton resonance is presumed to be overlapping with the aromatic phenyl resonances. This upfield shift for complex 2 indicates a more electron rich pyridine ring than when there is a proton or chloro-substituent. Additionally, for complex 2 a peak at 3.65 ppm with an integration equivalent to three protons confirms the presence of the methoxy group. There is not a significant shift observed in the ³¹P{¹H} NMR spectra for complex 1 and 2 compared to previously reported complex 3, and all three complexes showed two doublets around 56 ppm and 40 ppm with a ${}^{2}J_{PP} = 37$ Hz (Table 3). Queiroz et al. performed a detailed NMR study showing

that the location of the ³¹P chemical shift is dependent on the corresponding *trans* ligand, which was later confirmed by DFT calculations. ^{10,12,28} Based on their analysis, the upfield resonance should correspond to the phosphorus atom that is *trans* to the pyridine ring; whereas, the resonance downfield is the phosphorus atom *trans* to the chloride. Calculations of ³¹P isotropic tensor values using the GIAO method are in qualitative agreement with those observed by experiment, confirming the phosphorus assignments (see below).

Table 3. Comparison of ³¹P NMR data for RuCl₂(dppb)(ampy-L).

Ligand	Trans-isomer	Cis-isomer 1
Ampy	42.5 (d) & 41.5 (d)	54.9 (d) & 40.1 (d)
(Complexes 6 & 3)	$^2J_{PP} = 38 \text{ Hz}$	$^2J_{PP} = 37 \text{ Hz}$
Ampy-Cl	43.4 (d) & 42.0 (d)	54.0 (d) & 40.3 (d)
(Complexes 4 & 1)	$^2J_{\rm PP} = 39~{\rm Hz}$	$^2J_{\rm PP} = 37~{\rm Hz}$
Ampy- OMe	43.2 (d) & 42.4 (d)	55.7 (d) & 40.4 (d)
(Complexes 5 & 2)	$^2J_{PP} = 39 \text{ Hz}$	$^2J_{PP} = 37 \text{ Hz}$

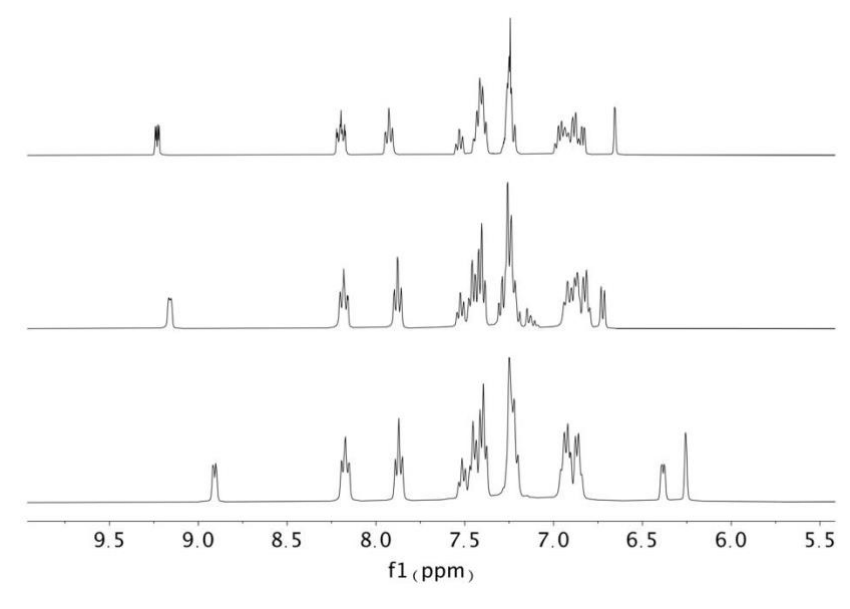


Figure 3. ¹H NMR spectrum of *cis*-RuCl₂(dppb)(ampy-Cl) (1, top), *cis*-RuCl₂(dppb)(ampy) (3, middle), *cis*-RuCl₂(dppb)(ampy-OMe) (2, bottom) in CD₂Cl₂.

In order to gain a better understanding of the effect of substitution at the *para*-position of the pyridine ring on the electron density of the metal center, cyclic voltammetry experiments were conducted. All three complexes exhibited quasi-reversible one-electron waves (Figure 4). The Ru(III/II) potential indicated the following trend in the overall donor ability of the ligands: ampy-Cl (0.217 V vs Fc^{0/+}) < ampy (0.184 V vs Fc^{0/+}) < ampy-OMe (0.165 V vs Fc^{0/+}). Thus, the oxidation potential of the complexes is directly related to the substitution group of the *para*-position of the pyridine ring. This trend is also observed for *cis*-RuCl₂(dppb)(4,4'-X₂-2,2'-bpy) complexes where the Cl-group (0.760 V vs Fc^{0/+}) is significantly less electron donating than the OMe-group (0.570 V vs Fc^{0/+}).²⁹ The Ru(III/II) potentials of complexes 1 and 2 differed by 0.052 V, thus supporting that substitution at the *para*-position of the pyridine ring has an effect on the electronic profile of the metal center. Furthermore, it supports our original hypothesis that there is a more subtle change in the electronic profile of the metal center with the alteration of only one *para*-substitution in comparison to disubstitution as in the case with bipyridine. (ampy-Y = 0.052 V vs. bpy: 0.190 V).

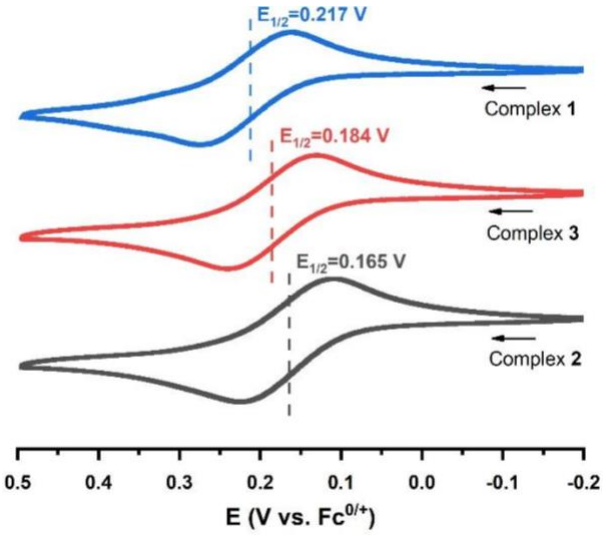


Figure 4. Cyclic voltammogram for *cis*-RuCl₂(dppb)(ampy-Cl) (1), *cis*-RuCl₂(dppb)(ampy) (3) and *cis*-RuCl₂(dppb)(ampy-OMe) (2). Measurements carried out in CH₂Cl₂ using [NBu₄][PF₆] (0.1 M) electrolyte with 1 mM of complex concentration and at scan rate of 100 mV s⁻¹. Potentials are in V referenced against Fc⁰/Fc⁺.

The electronic structures of complexes 1-3 were further characterized with DFT calculations. Redox potentials relative to Fc^0/Fc^+ were calculated using the M06 functional and found to be in reasonable agreement with cyclic voltammetry experimental data $(\Delta E_{1/2}^{(1\to 3)} = 0.05 \text{ V}; \Delta E_{1/2}^{(2\to 3)} = -0.03 \text{ V}; \Delta E_{1/2}^{(1\to 2)} = 0.08)$ (Table S4 and S5). The highest occupied molecular orbital (HOMO) for all complexes is d_{xy} in character with π^* interactions with the chloride ligands (Figure 5). The next two occupied orbitals, HOMO–1 and HOMO–2, are d_{xz} and d_{yz} with π^* interaction to a single chloride in each case. The lowest unoccupied molecular orbital (LUMO) is primarily pyridine π^* in character with a very small amount of the unfilled d_{z2} orbital character. Higher lying LUMOs feature significant delocalization at the Ru and ampy ligand.

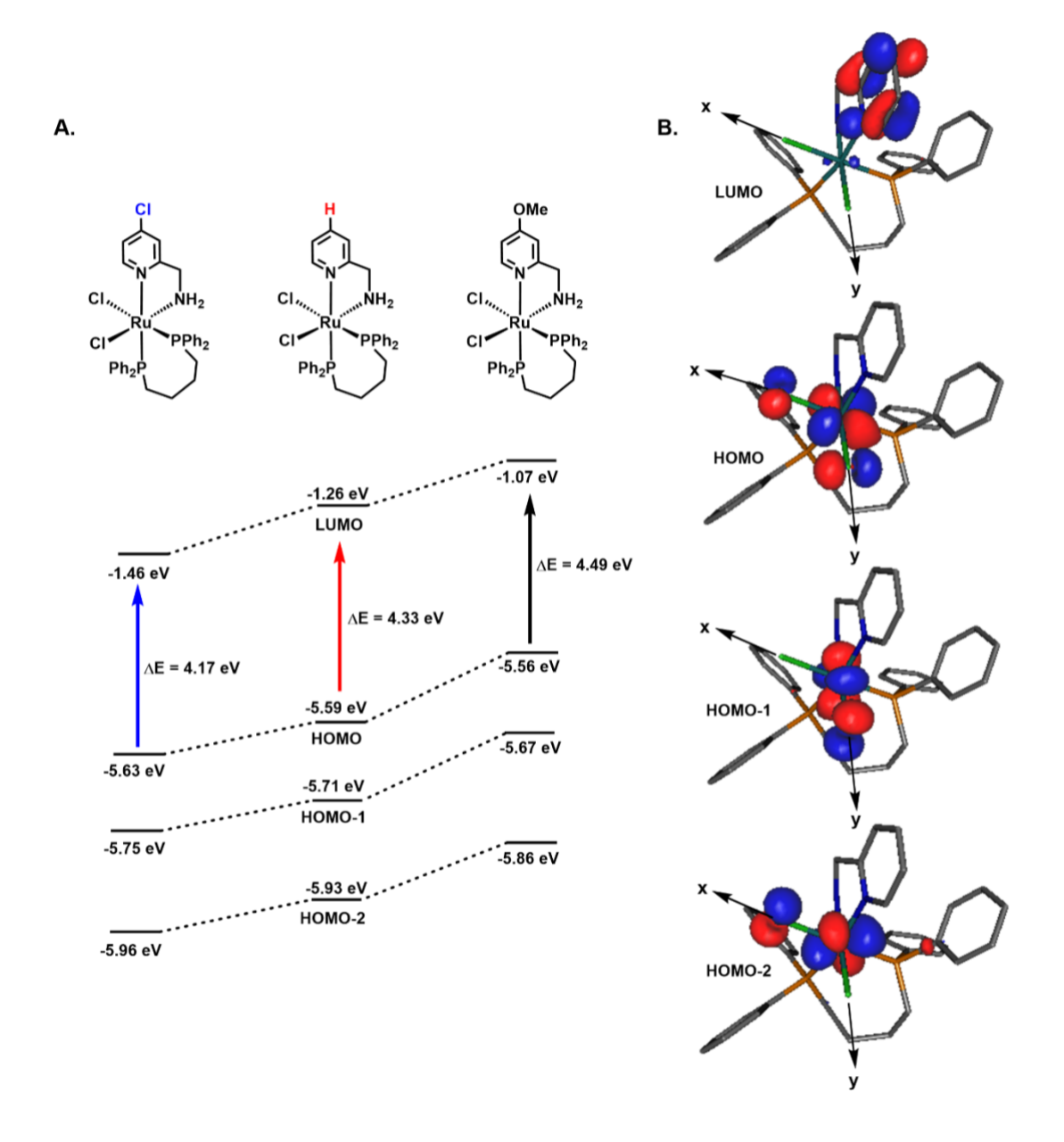


Figure 5. A) Frontier orbitals and the associated energies of complexes 1, 2, and 3. B) Visualization of molecular orbitals for complex 3.

The UV-Vis spectra of all three complexes show intense bands at <330 nm and 353 - 365 nm (Figure 6). These peaks have been observed in the literature for other Ru(dppb)(2,2'-bipy) and Cu(ampy) complexes.^{29,30} The peak less than 330 nm can be related to the ligand to ligand charge transfer from the substituted amino-pyridine ligand.^{31,32} The higher wavelength bands can be

assigned to charge transfer transitions ($Ru(II)d_{\pi\to\pi^*}$). Time-dependent DFT calculations are consistent with this assignment. The most intense transitions in the 350-365 nm range are composed of HOMO-2 (cf., Figure 5) to multiple LUMO levels (Figure S24). Since these transitions occur from metal-based d orbitals, increased electron donation from the ampy-L ligand leads to blueshifted transitions.

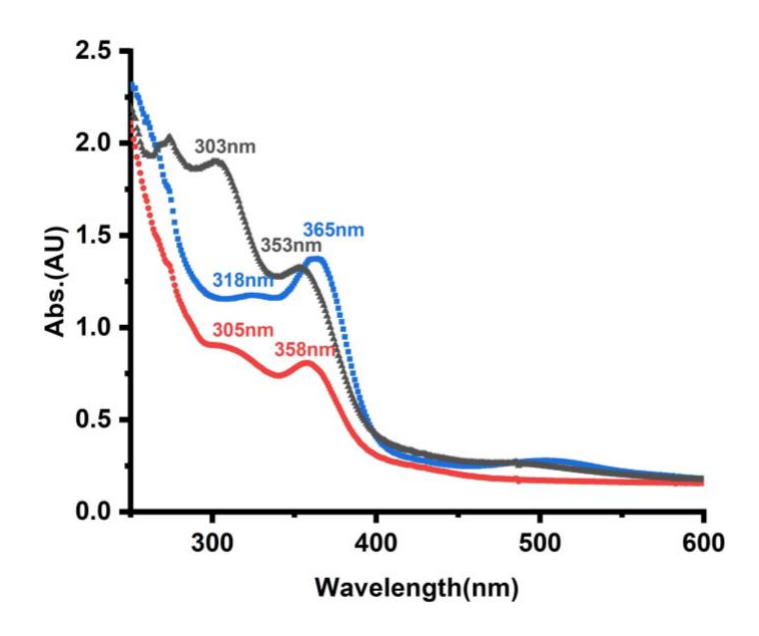


Figure 6. UV-vis spectra in CH₂Cl₂ (0.3 mM) of complex **1** (blue line), complex **2** (black line) and complex **3** (red line).

Catalytic Transfer Hydrogenation of Ketones

Ru(II) complexes containing phosphine and diamine ligands have been published as successful catalyst for hydrogenation of ketones.^{33–35} Specially related to our complexes, RuCl₂(dppb)(ampy) has previously been reported to have high catalytic activity for transfer hydrogenation of ketones (Scheme 2).¹⁰ Moreover, a previous published study showed that Ru(II) complexes with more electron rich metal centers typically yield higher rates of catalytic transfer

hydrogenations.³⁴ Catalysis was probed with complexes **1** and **2** to determine if changing the electronic profile of the metal center had an similar impact on catalytic activity.

Scheme 2. Generic Scheme of Transfer Hydrogenation of Ketones

Transfer hydrogenation reactions were conducted between several ketones and the hydrogen donor, 2-propanol, with complexes 1 and 2 and NaOH. The relative ratio of substrate:Ru:NaOH was 2000:1:40 used was identical to the conditions previously reported to achieve an ideal replication and comparison.¹⁰ Complexes 1 and 2 were observed to be as catalytically robust as previous reported complex 3 with substrates 1-(4-chlorophenyl)ethan-1-one, (E)-4-phenylbut-3-en-2-one, and benzophenone. All reactions gave quantitative to near quantitative yields (by ¹H NMR spectroscopy based on an internal standard) in short reaction times (c.a. 4 min). Complexes 1 and 2 were also found to be selective for the carbonyl compared to the alkene when an unsaturated ketone was utilized. Although, there was no significant difference in the overall final yield between the three complexes, it was unknown if a difference in the rate of catalysis could be observed. To determine if the subtle difference in electronics of the Ru-center impact the rate of catalysis, we measured a turn-over-number (TON) and an estimated single point turn-over-frequency at 1 minute for catalysis with benzophenone, using conditions and protocols previously reported for similar catalysts. Due to the potential error that could occur with a one minute time point, kinetics were attempted with increased substrate concentration and decreased catalyst loading (20000:1:40 or 4000:1:40) in an attempt to slow the rate of the reaction.

Unfortunately, this approach led to inconsistent results and incomplete reaction yields. Additionally, attempts to slow the reaction speed by lowering the temperature still did not provide a method to collect consistent data at longer intervals. Nonetheless, using the TON at 1 min does suggest a subtle different in the rate of catalysis was observed between the three complexes, with 2 having the highest TOF (89,400 h⁻¹). A pattern that agrees with the previous observed increase in rate for more electron rich metal centers. However, a extensive and detailed studies would need to be completed to draw any definite conclusions.

Table 4. Catalytic Transfer Hydrogenation of Ketones using *cis*-RuCl₂(dppb)(ampy-L).

Ketone	Product	Complex 1	Complex 2	Complex 3
CI	CI	100 (4)	88 (4)	100 (4)
	OH	96 (4)	94 (4)	92(4)
	OH	91 (5) TOF = 73,200 h ⁻¹	95 (2) TOF = 89,400 h ⁻¹	98 (10) ^a TOF = 69,600 h ⁻¹

Conditions: 0.1 M ketone in 2-propanol, ketone:Ru:NaOH = 2000:1:40. Stated yields are by ¹H NMR with respect to an internal standard. Turnover frequency (moles of ketone converted to alcohol per mole of catalyst per hour) at one minute. ^aPreviously reported in reference 10.

B. Synthesis and characterization of trans-RuCl2(dppb)(ampy-L)

The complexes **4** and **5**, *trans*-RuCl₂(dppb)(ampy-L) (L = Cl or OMe) were synthesized in a similar manner as previously reported for *trans*-RuCl₂(dppb)(ampy) (**6**). The reaction between RuCl₂(dppb)PPh₃ and ampy-L (L = Cl or OMe) in the dark at room temperature provided pure complexes (Scheme 3). However, due to the increased solubility for complexes **4** and **5**, an

alternative isolation process was utilized than previously published. Specifically, for complex **5** the reaction mixture was concentrated to dryness, the solid was suspended in diethyl ether and collected on a frit. Unlike the large separation of the doublets in the ³¹P NMR spectra for complexes **1** and **2**, the *trans*-complexes exhibited two doublets at c.a. 42 ppm that were closer together resulting in significant leaning.

Scheme 3. Synthesis of *trans*-RuCl₂(dppb)(ampy-L).

In order to understand the difference in the electrochemistry of the *trans*-complexes compared to the *cis*-complexes, cyclic voltammetry studies under the same conditions described above were performed (Figure 7). Unlike the *cis*-complexes, the *trans*-complexes interestingly did not show well-behaved redox behavior (i.e., reversible or quasi reservable events). However, the trend was seen for the *trans*-RuCl₂(dppb)(ampy-L) complexes was similar to their *cis* isomers in the anodic current (E_a). Moreover, all of the *cis*-complexes show higher oxidation potentials ranging from approximately 34 mV to 112 mV greater than their respective *trans*-isomers. These anodic shifts upon isomerization are well documented for Ru(II) chemistry.²⁹

The electronic structure of complexes **4-6** are also similar with a Ru-based d_{xy} HOMO and pyridine-based π^* LUMO (Figure S27), and a more pronounced blueshift is seen in the electronic spectrum ($\lambda = 333$ vs. 398 nm for **5** and **4**, respectively, Figure 8) that is consistent with larger frontier molecular orbital energy differences for the trans relative to the cis complexes. TD-DFT calculations indicate the most intense transitions in the case of complexes **4** and **6** in the 380-400

nm range (cf., Figure 7) are composed of HOMO-1 and HOMO to LUMO and LUMO+2 (Figure S28). Similarly, the most intense transition for complex **5** at 333 nm consists of significant HOMO-2, HOMO-1, and HOMO contributions to LUMO and several LUMO+*n* states.

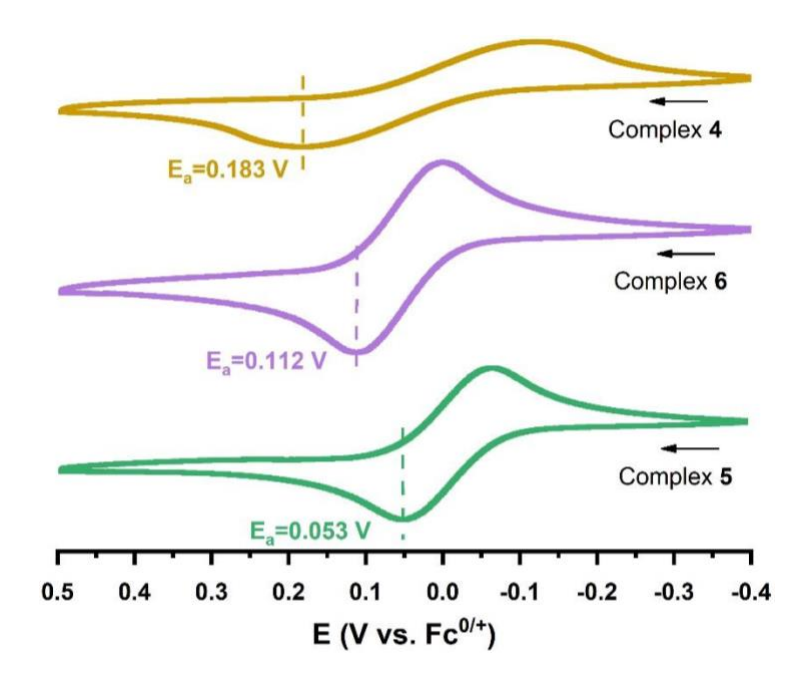


Figure 7. Cyclic voltammogram for *trans*-RuCl₂(dppb)(ampy-Cl) (4), *trans*-RuCl₂(dppb)(ampy) (6) and *trans*-RuCl₂(dppb)(ampy-OMe) (5). Measurements carried out in CH₂Cl₂ using [NBu₄][PF₆] (0.1 M) electrolyte with 1 mM of complex concentration and at scan rate of 100 mV s⁻¹. Potentials are in V referenced against Fc⁰/Fc⁺.

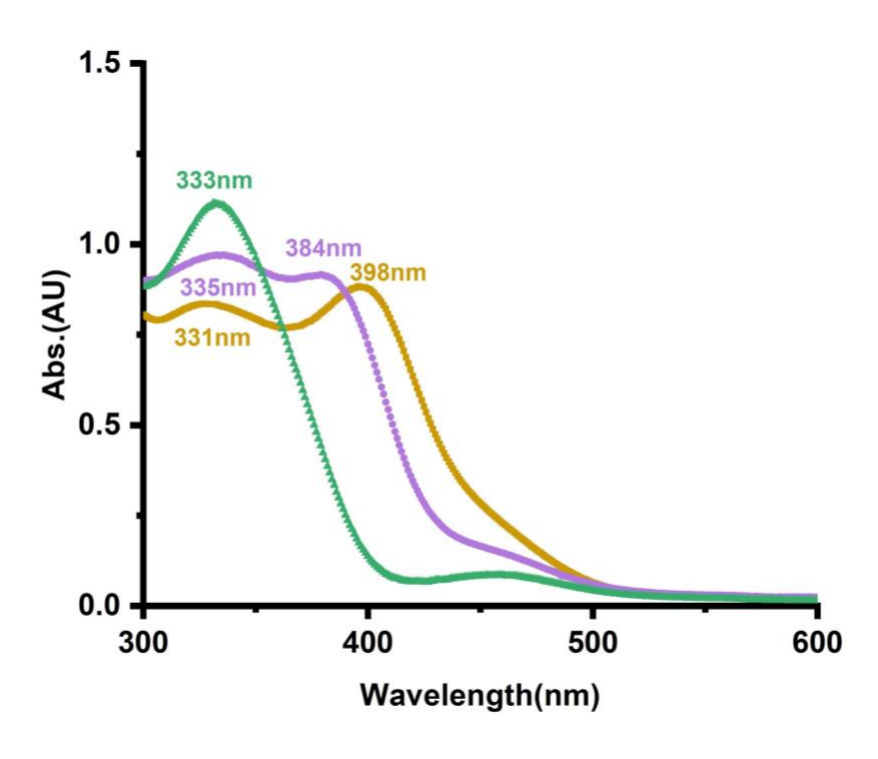


Figure 8. UV-vis spectra in CH₂Cl₂ (0.3 mM) of Complex 4 (gold line), Complex 5 (green line) and Complex 6 (purple line).

Previous publications have demonstrated that [RuCl₂(dppb)(N-bichelates)] complexes isomerize from a *trans*-configuration to their *cis*-isomers under the correct conditions. Specifically, [RuCl₂(dppb)(4,4'-X₂-2,2'bipy)] complexes isomerize in the presence of heat and light (Scheme 4).²⁹ Santiago and coworkers observed a noticeable difference in the rate of isomerization for [RuCl₂(dppb)(4,4'-X₂-2,2'bipy)] based on the electron density at the metal center, where the more electron rich metal centers would isomerize more rapidly than electron deficient metals.²⁹ NMR and UV-Vis experiments were conducted on all three *trans* complexes to gain a better understanding of how electron density impacts the rate of isomerization from the *trans*-complexes to the *cis*-isomer 1 complexes (Figure 9, Figure 10). Upon exposure to light and heat, the complexes isomerize exclusively to the more stable *cis*-isomer 1 under conditions we have explored. A UV-Vis spectrum was collected every 10 minutes while the sample was exposed to white light and heated to 308 K. As seen in Figure 9, there is a single isosbestic point indicating

that the final product, *cis*-RuCl₂(dppb)(ampy) (3), is the only product formed. The clean conversion from the *trans*-isomer to the *cis*-isomer was also observed for complexes 4 and 5 (Figures S9, S11, S13, and S14). Additionally, experiments were conducted to confirmed that the *trans*-complex does not convert to the *cis* form at an appreciable rate at room temperature and at 308 K in complete darkness; supporting previous findings that such a process requires the presence of light. (Figures S18, S19, S20).

The rate of isomerization of each of the complexes was determined using ¹H NMR spectroscopy (Figure 10). An NMR tube with trans-complex (6) was heated to 308 K in the presence of white light. The reaction was followed by the disappearance of the trans-orthoresonance at 8.82 ppm and the appearance of cis-ortho-resonance at 9.16 ppm. The rates of isomerization were determined by plotting [cis-Ru] vs time (Table 5), where the concentration of Ru was calculated from the integration of the value for the *ortho-H* versus an internal standard in the ¹H spectrum (Figure 11). The rates for the appearance and disappearance of each isomer were in strong agreement for complex 4 and 6. However, for complex 5 the rates were different and upon further probing it was determined that the complex was susceptible to decomposition after prolonged heating in dichloromethane. The rate of isomerization for complex 5 was studied at lower concentrations by UV-Vis in both toluene and dichloromethane and the rate of disappearance and appearance were in agreement. Unlike the Ru(dppb)(bpy) complexes, we did not see a change in the rate due to the difference in electron density. Mechanistic studies on the Ru(dppb)(bpy) systems indicate the isomerization is likely proceeding through a twisting mechanism and main driving force for the isomerization process is related to the Ru-Cl bond character which is directly impacted by the ligands a metal center.²⁹ Based on the X-ray crystallography data for our three complexes no significant difference in Ru-Cl bond length were

observed thus supporting the lack of differences in rate of isomerization. Therefore, we hypothesize that the subtle difference in the electron density must be more significant to impact the Ru-Cl bond character and consequently the rate of isomerization.

Scheme 4. Isomerization of *trans*-RuCl₂(dppb)(ampy-L) to *cis*-RuCl₂(dppb)(ampy-L) with heat in the presence of light.

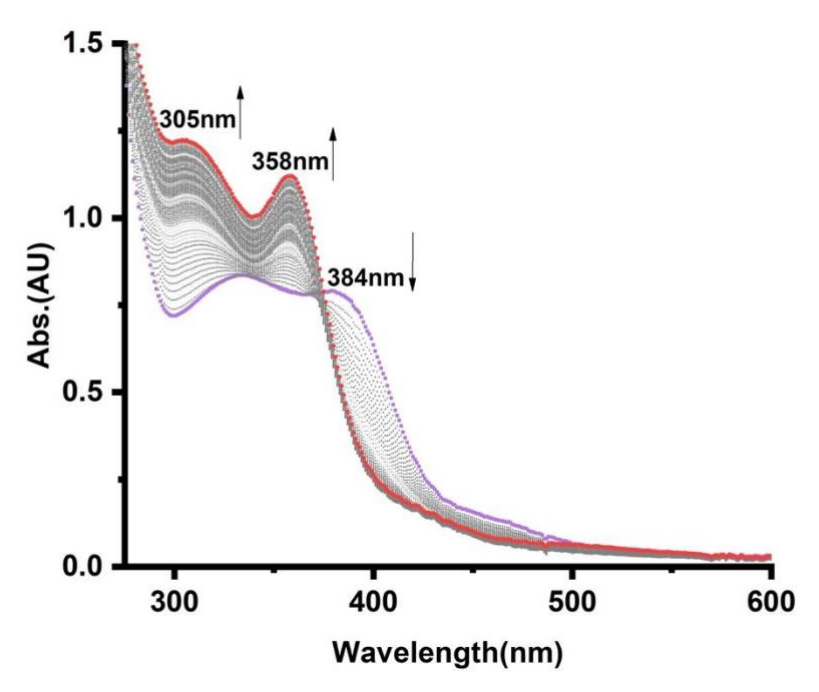


Figure 9. Photoisomerization process under white light of *trans*-RuCl₂(dppb)(ampy) (complex **6**, purple line) to *cis*-RuCl₂(dppb)(ampy) (complex **3**, red line) in CH₂Cl₂ solution (0.25 mM) at 308 K.

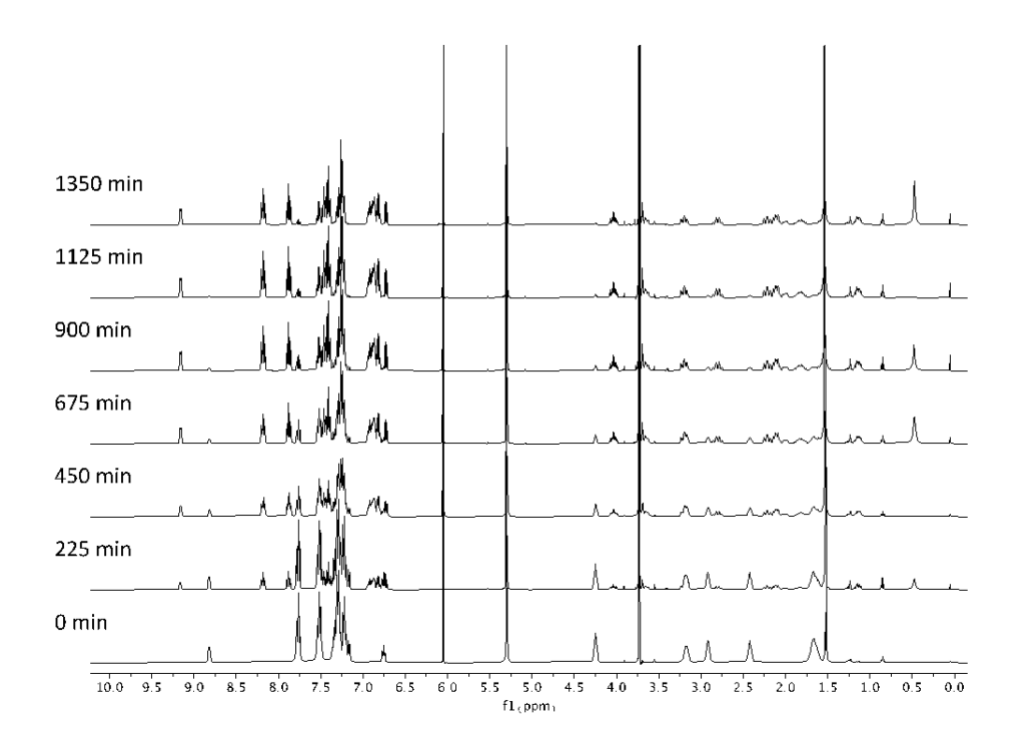


Figure 10. Photoisomerization of *trans*-RuCl₂(dppb)(ampy)(6) to *cis*-RuCl₂(dppb)(ampy) (3) in the presence of light monitored at 308 K by ¹H NMR Spectroscopy (CD₂Cl₂, r.t., external standard: 1,3,5- trimethxoybenzene 6.05 ppm and 3.73 ppm)

Table 5. Isomerization rate constant data of *trans*-RuCl₂(dppb)(ampy-L) to *cis*-

RuCl₂(dppb)(ampy-L) with heat in the presence of light

Ligand	Isomerization Rate Constant of Disappearance of <i>trans</i> -product (min ⁻¹)
Ampy-H	0.00193(2)
Ampy-Cl	0.00190(7)
Ampy-OMe	0.0016(3)

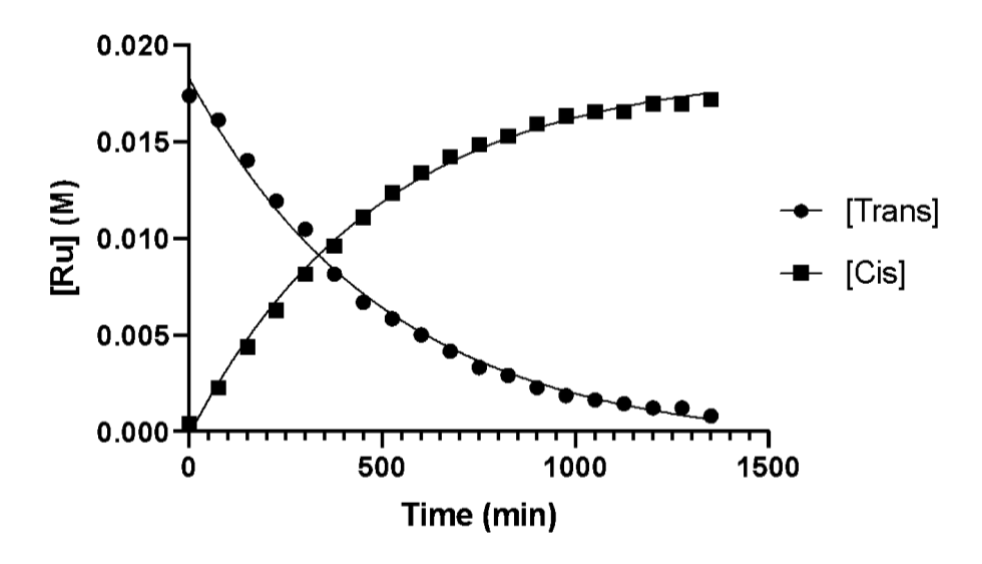


Figure 11. First order plots for the isomerization of *trans*-RuCl₂(dppb)(ampy) (6) to *cis*-RuCl₂(dppb)(ampy) (3) at 308 K.

Conclusions

In summary, we have demonstrated that four ruthenium (II) complexes: *cis*-RuCl₂(dppb)(ampy-Cl) (1), *cis*-RuCl₂(dppb)(ampy-OMe) (2), *trans*-RuCl₂(dppb)(ampy-Cl) (4), *trans*-RuCl₂(dppb)(ampy-OMe) (5) can be prepared in high yield from [RuCl₂(PPh₃)₃] or [RuCl₂(dppb)(PPh₃)]. The replacement of a second substituted pyridine by an amine (bipyridine versus aminopyridine) yields a more subtle change in the electronic density around the metal center This subtle difference is observable via cyclic voltammetry changes as well as by the expected shifts in peaks seen in UV-Vis and NMR spectroscopy. X-ray crystallography showed only small changes in the bond angles or bond distances across the series, suggesting that electronic density changes at the metal does not generates significant structural differences.

These complexes provided an opportunity to explore if the subtle change in the electron density of the metal center impacts catalysis and *trans/cis* isomerization. The complexes were probed as potential catalysts for the selective reduction of ketones to alcohols through transfer hydrogenation. All three of the *cis* complexes are capable of catalysis, with quantitative or near

quantitative conversion to the desired product. Additionally, catalytic transfer hydrogenation reactions are conducted in short time frames (> 5 min). A subtle difference in the rate of hydrogenation (TOF) at 1 minute is observed for 2, the most electron rich complex. Although, a potential subtle change in the rate of hydrogenation was observed, the slight changes in the metal center's electron density are not significant enough to cause a difference in the rates of isomerization. Lastly, *trans-cis* isomerization of these complexes confirmed that the *cis* complexes is favored under our general conditions, as the *trans* complexes fully isomerizes to its *cis* isomer under in the presence of light and heat. Future exploration of other derivatives and more detailed mechanistic studies are underway in hopes of improving the overall possible catalysis of complexes such as these.

Experimental Section

General Methods. Unless otherwise noted, all synthetic procedures were performed under anaerobic conditions in a nitrogen-filled glovebox or by using standard Schlenk techniques. Toluene- d_3 , methylene chloride- d_2 and chloroform- d_1 were stored under a N₂ atmosphere. ¹H NMR, ¹³C{¹H} NMR (operating frequency 125 MHz) and ³¹P{¹H} NMR (operating frequency 121 MHz) spectra were recorded on a JEOL ECS 400 MHz spectrometer. All ¹H and ¹³C{¹H} NMR spectra are referenced against residual proton signals (¹H NMR) or the ¹³C resonances of the deuterated solvent (¹³C{¹H} NMR). UV-vis data was obtained using a Hewlett Packard 8454 diode array spectrophotometer with a scan range from 200 nm to 1100 nm in a 10 mm path quartz cell. The spectrometer was equipped with HP Chemstation software and a Unisoku cryostat to provide needed heat (308 K) for the photoisomerization experiments. Electrochemical measurements were carried out on a model 620E Electrochemical Workstation (CH Instruments).

3 mL of a dichloromethane solution of the Ru complexes (1 mM) containing 0.1 M of [NBu4][PF6] were prepared in the glovebox and were transferred to an electrochemical cell outside the glovebox, which has been purged with Ar for 10 minutes (note: a conventional three-electrode cell was used with a glassy carbon working electrode, an Ag/AgNO3 (0.01 M) and a platinum wire as the counter electrode). The potentials were measured with respect to the Ag/AgNO3 reference electrode and converted to Fc^{0/+} (Fc^{0/+} potential measured under the same experimental conditions). Cyclic voltammograms were obtained under an Ar atmosphere at a scan rate of 100 mV/s. For the *trans* isomers, the CV cell and syringe were covered with Al foil to prevent the exposure to light. The preparation, isolation and characterization of RuCl₂(PPh₃)₃³⁶, (4-chloropyridin-2-yl)methylamine³⁷, 5-(butylamino)pentan-1-ol³⁸, *cis*-RuCl₂(dppb)(ampy)¹⁰ and *trans*-RuCl₂(dppb)(ampy)¹⁰ have been previously reported. 2-(aminomethyl)pyridine (ampy), diphenylphosphinobutane (dppb) and other reagents were obtained from a commercial source and used as received unless otherwise indicated. All solvents were purchased as anhydrous solvents and used as received.

X-ray Crystallography Crystals suitable for structural analysis were grown by diffusion of pentane into chloroform. The samples were suspended in mineral oil at ambient temperature, mounted on a MiTeGen Micromount and transferred to a Bruker AXS SMART APEXII CCD X-ray diffractometer. The X-ray diffraction data were collected at 100(2) K using Mo-K α (λ = 0.71073 Å) radiation. The frames were integrated with the Bruker SAINT software package using a narrow-frame algorithm. The data was corrected for absorption effects using the Multi-Scan method (SADABS).³⁹ Structures were solved and refined using the SHELXTL Software Package,⁴⁰ and molecular diagrams were generated using X-SEED.^{41,42} Table 1 summarizes the

data collection and refinement parameters for the structures reported in this manuscript. Additional structural data is reported in the supplementary information and can be accessed from the CCDC.

(4-methoxy-pyridin-2-yl)methylamine. This compound has been previously published but a modified procedure was conducted.³⁷ (4-methoxypyridin-4-yl)methanol (1.0 g, 7.19 mmol) and triphenylphosphine (5.65 g, 21.56 mmol) were added to a Schlenk flask and placed in an ice bath under nitrogen. Cold anhydrous THF (26 mL) was added by syringe and the reaction was stirred for 10 minutes. DIAD (2.12 mL, 10.78 mmol) was added dropwise over 10 minutes to the reaction flask and the solution became a light orange. The same process was repeated adding diphenylphosphoroylazide (1.45 mL, 8.62 mmol) and a white solid precipitated out of the solution. The reaction was left to stir overnight under nitrogen in the ice bath and allowed to warm to ambient temperature. The reaction flask was then removed from the dewar and warmed to room temperature over an hour. After warming, the reaction was stirred and heated to 55 °C for an hour. RO water (5 mL) was added and the reaction was stirred and heated to 55 °C for an hour and then concentrated down on the Schlenk line. The residue was dissolved in dichloromethane (45 mL) and RO water (45 mL) and placed in a separation funnel. The pH of the aqueous layer was adjusted to a pH of 3 with H₂SO₄. The dichloromethane layer was drained, and an additional 45 mL of dichloromethane was added to wash the aqueous layer. The pH of the aqueous layer was brought to a pH of 12 with NaOH and extracted three times with dichloromethane (3 x 45 mL). The three extraction layers were dried with Na₂SO₄ and concentrated the solution down to yield an orange oil and solid. The produce was columned on silica gel using a 300:30:1 CHCl₃:CH₃OH:NH₃ eluent. The characterization data matches previously published.

cis-RuCl₂[Ph₂P(CH₂)₄PPh₂](ampy-Cl) (1). Method 1: RuCl₂(PPh₃)₃ (0.300 g, 0.310 mmol) and toluene (4.5 mL) was added to (4-chloro-pyridin-2-yl)methanamine (0.530 g, 0.370 mmol), and stirred for 1 hour. 1,4-bis(diphenylphosphino)butane (0.130 g, 0.310 mmol) was added to the solution and the reaction was refluxed overnight. The reaction was cooled to room temperature and a yellow solid was obtained by vacuum filtration, washed with diethyl ether, and dried under vacuum (0.179 g, 78%). **Method 2:** RuCl₂(dppb)(PPh₃) (0.265 g, 0.306 mmol) was dissolved in toluene (4 mL) in a round bottom flask. (4-chloro-pyridin-2-yl)methylamine (0.052 g, 0.366 mmol) was dissolved in toluene (2 mL) and was added to the reaction flask to form a brown-green heterogenous mixture. The mixture was refluxed overnight and then allowed to cool to room temperature. A yellow precipitate was collected by vacuum filtration, washed with pentane and dried under vacuum (0.171 g, 76%). ¹H NMR (400 MHz, CDCl₃): 9.24 (m, 1H; o-C₅H₃N), 8.17 (m, 2H; aromatic protons), 7.92 (t, ${}^{3}J_{HH} = 8$ Hz, 2H; aromatic protons), 7.57-6.81 (m, 17H; aromatic protons, C₅H₃N), 6.66 (s, 1H; C₅H₃N), 4.09 (m, 1H; CH₂), 3.72 (m, 2H; NH₂), 3.21 (m, 1H; CH₂), 2.83 (m, 1H; CH₂), 2.40-0.90 (m, 7H; CH₂). ¹H NMR (400 MHz, CD₂Cl₂) δ 9.07 (m, 1H, o-C₅H₃N), 8.19-6.85 (m, 21H, aromatic protons), 6.75 (s, 1H, C₅H₃N), 4.01 (m, 1H, $P(CH_2)_4P$), 3.70 (m, 2H, NH₂) 3.16 (m, 1H, CH₂N), 2.80 (m, 1H, P(CH₂)₄P), 2.31-1.10 (m, 7H, $P(CH_2)_4P$, NH₂). ¹³C{¹H} NMR (101 MHz, CD₂Cl₂) δ 159.09 (s, NCCH₂, of C₅H₃N), 151.54 (s, CH of C₅H₃N), 143.65 - 126.92 (m, aromatic carbons), 34.40 (d, ${}^{1}J_{CP} = 27$ Hz, CH₂P), 29.15 (d, ${}^{1}J_{CP} = 30 \text{ Hz}, \text{CH}_{2}\text{P}), 27.19 \text{ (s, CH}_{2}\text{CH}_{2}\text{P}) 19.24 \text{ (s, CH}_{2}\text{CH}_{2}\text{P}).} {}^{31}\text{P}\{{}^{1}\text{H}\} \text{ NMR (162 MHz, CDCl}_{3}):$ δ 54.02 (d, ${}^{2}J_{PP}$ = 37 Hz), 40.74 (d, ${}^{2}J_{PP}$ = 37 Hz). UV-Vis (CH₂Cl₂) λ_{max} [nm] (ε x 10⁻³ M⁻¹, cm⁻¹) 365 (3.5), 502 (0.6). CV (CH₂Cl₂, 100 mV) $E_{1/2} = 0.217$ V. Anal. Calc'd. for C₃₄H₃₅Cl₃N₂P₂Ru•CHCl₃: C, 48.84; H, 4.22; N, 3.26 Found: C, 48.84; H, 4.16; N, 3.25.

cis-RuCl₂[Ph₂P(CH₂)₄PPh₂](ampy-OMe) (2). Method 1: (4-methoxypyridin-2-yl)methanamine (0.510 g, 3.70 mmol) was added to a Schlenk flask and dissolved in toluene (4.5 mL). [RuCl₂(PPh₃)₃] (0.300 g, 0.31 mmol) was added to the flask, and the tan solution was left to stir for 1 hour. 1,4-bis(diphenylphosphino)butane (0.130 g, 0.310 mmol) was added to the reaction and the reaction was refluxed overnight. The solution turned a yellow green color. The reaction was cooled to room temperature and a bright yellow solid was collected by vacuum filtration, washed with diethyl ether, and dried under vacuum (0.180 g, 81%). Method 2: (4-methoxypyridin-2-yl)methanamine (0.024 g, 0.174 mmol) was added to a Schlenk flask. RuCl₂(dppb)(PPh₃) (0.125 g, 0.145 mmol) was added to the reaction flask and dissolved in toluene (3.0 mL) and refluxed for 20 hours in light. The reaction was cooled to room temperature and the yellow precipitate was collect on a fine porosity frit, washed with diethyl ether and left to dry under vacuum (0.063 g, 59%). H NMR (400 MHz, CD₂Cl₂) δ 8.90 (m, 1H, o-C₅H₃N), 8.26 – 6.70 (m, 20H, aromatic protons), 6.37 (m, 1H, m-C₅H₃N) 6.25 (d, ${}^{4}J_{HH} = 3$ Hz, 1H, m-C₅H₃N), 4.01 (m, 1H, P(C H_{2})₄P), 3.73 - 3.57 (m, 5H, overlap of OCH₃, CH₂N, NH₂), 3.14 (m, 1H, CH₂N), 2.78 (m, 1H, P(CH₂)₄P), 2.35 - 1.10 (m, 7H, P(CH₂)₄P, NH₂). ¹³C{¹H} NMR (101 MHz, CD₂Cl₂) δ 165.51 (s, C(OMe) of C_5H_3N), 158.64 (s, NCCH₂ of C_5H_3N), 151.40 (s, CH of C_5H_3N), 141.28 – 106.27 (m, aromatic carbons), 55.59 (s, OCH₃), 34.49 (d, ${}^{1}J_{CP} = 27 \text{ Hz}$, CH₂P), 29.32 (d, ${}^{1}J_{CP} = 30 \text{ Hz}$, CH₂P), 27.25 (s, CH₂CH₂P) 19.30 (s, CH₂CH₂P). 31 P{ 1 H} NMR (162 MHz, CD₂Cl₂): δ 55.20 (d, 2 J_{PP} = 37 Hz, dppb), 40.84 (d, ${}^{2}J_{PP} = 37 \text{ Hz}$, dppb). UV-Vis (CH₂Cl₂) λ_{max} [nm] ($\epsilon \times 10^{-3} \text{ M}^{-1} \text{ cm}^{-1}$) 353 (3.93), 486 (0.442). CV (CH₂Cl₂, 100 mV) $E_{1/2} = 0.165$ V. Anal. Calcd. for C₃₅H₃₈Cl₂N₂OP₂Ru·0.5H₂O: C, 56.38; H, 5.27; N, 3.76. Found: C, 56.31; H, 5.23; N, 3.88.

cis-RuCl₂[Ph₂P(CH₂)₄PPh₂](ampy) (3). The complex was synthesized by the previously published method. The characterization data was in agreement with previously published data.²⁵ UV-Vis (CH₂Cl₂) λ_{max} [nm] (ϵ x 10⁻³, M⁻¹ cm⁻¹) 305 (3.05), 358 (2.94) CV (CH₂Cl₂, 100 mV) $E_{1/2} = 0.184 \text{ V}$.

trans-RuCl₂[Ph₂P(CH₂)₄PPh₂](ampy-Cl) (4). RuCl₂(dppb)(PPh₃) (0.350 g, 0.370 mmol) was dissolved in dichloromethane (5 mL). (4-chloro-pyridin-2-yl)methylamine (ampy-Cl) (0.081 g mg, 0.620 mmol) dissolved in dichloromethane (1 mL) and added dropwise to the stirring solution of RuCl₂(dppb)(PPh₃). The reaction was stirred at room temperature for 1 hour in the dark. The solution slowly turned from dark green to dark yellow, and the resulting solution was filtered through celite. The reaction mixture was concentrated in vacuo to approximately 3 mL. Pentane (c.a. 6 mL) was added slowly and the reaction mixture was left to stir for 10 minutes. The yellow solid was collected on a fine frit, washed with diethyl ether (3 mL) and dried under vacuum (0.160 g, 52%). ¹H NMR (400 MHz, CD₂Cl₂) δ 8.67 (s, 1H, C₅H₃N), 7.75-7.18 (m, 21H; aromatic protons), 6.77 (s, 1H; C5H3N), 4.23 (m, 1H; C5H3N), 4.21 (m, 2H; NH2), 3.18 (m, 1H; CH2), 2.91(m, 1H; CH₂), 2.44-1.66 (m, 7H; CH₂). ¹³C{¹H} NMR (101 MHz, CD₂Cl₂) δ 165.20 (NCCH₂) of C₅H₃N), 155.70 (CH of C₅H₃P), 144.31-121.11 (m, aromatic carbons), 49.72 (s, CH₂N), 32.17 $(d, {}^{1}J_{CP} = 30 \text{ Hz}, CH_{2}P), 25.43 \text{ (s, } CH_{2}CH_{2}P), 23.99 \text{ (d, } {}^{1}J_{CP} = 27.5 \text{ Hz, } CH_{2}P), 19.80 \text{ (s, }$ CH₂CH₂P). ${}^{31}P\{{}^{1}H\}$ NMR (162 MHz, CD₂Cl₂) δ 43.10 (d, ${}^{2}J_{PP}$ = 38 Hz), 41.79 (d, ${}^{2}J_{PP}$ = 38 Hz). UV-Vis (CH₂Cl₂) λ_{max} [nm] (ϵ x 10⁻³, M⁻¹ cm⁻¹) 331 (2.90), 398 (2.66) CV (CH₂Cl₂, 100 mV) E_{ap} = 0.183 V. Anal. Calc'd. for C₃₄H₃₅Cl₃N₂P₂Ru•0.5CH₂Cl₂: C, 52.89; H, 4.63; N, 3.58 Found: C, 52.50; H, 4.63; N, 3.69.

trans-RuCl₂[Ph₂P(CH₂)₄PPh₂](ampy-OMe) (5). (4-methoxypyridin-2-yl)methanamine (0.061 g, 0.44 mmol) was dissolved in dichloromethane (6 mL) and added dropwise to RuCl₂(dppb)(PPh₃) (0.230 g, 0.370 mmol). The reaction was stirred at room temperature in the dark for 1.5 hours, and the solution turned from dark green to yellow. The solution was filtered through celite and reduced by vacuum to dryness. Diethyl ether was added to the remaining solid. The precipitate was collected via vacuum filtration on a frit, washed with diethyl ether and left to dry under vacuum (0.157 g, 52%). ¹H NMR $(400 \text{ MHz}, \text{CD}_2\text{Cl}_2) \delta 8.58 \text{ (dd, }^3J_{\text{HH}} = 6.6 \text{ Hz}, J_{\text{HH}} = 3 \text{ Hz}, 1\text{H}, o\text{-C}_5H_4\text{N})$, 7.76 - 7.15 (m, 20H, aromatic protons), 6.69 (d, ${}^{4}J_{HH} = 3$ Hz, 1H, C₅H₄N), 6.32 (dd, ${}^{3}J_{HH} = 6.7$, $^{4}J_{HH} = 3 \text{ Hz}, 1H, C_{5}H_{4}N), 4.17 \text{ (pseudo t}, ^{3}J_{HH} = 6.3 \text{ Hz}, 2H, NC}H_{2}), 3.74 \text{ (s}, 3H, OC}H_{3}), 3.15 \text{ (m},$ 2H, $P(CH_2)_4P$), 2.91 (m, 2H, NH_2), 2.39 (m, 2H, $P(CH_2)_4P$), 1.74 – 1.45 (m, 4H, $P(CH_2)_4P$). 13 C{ 1 H} NMR (101 MHz, CD₂Cl₂) δ 165.87 (s, C(OMe) of C₅H₃N), 164.94 (NCCH₂ of C₅H₃N), 155.76 (CH of C₅H₃N), 138.60 - 106.74 (m, aromatic carbons), 55.64 (OCH₃), 49.93 (s, CH₂N), 32.97 (d, ${}^{1}J_{CP} = 29$ Hz, $CH_{2}P$), 25.69 (s, $CH_{2}CH_{2}P$), 24.29 (d, ${}^{1}J_{CP} = 27$ Hz, $CH_{2}P$), 19.69 (s, CH₂CH₂P). ${}^{31}P{}^{1}H{}$ NMR (162 MHz, CD₂Cl₂) δ 43.23 (d, ${}^{2}J_{PP}$ = 38 Hz), 42.38 (d, ${}^{2}J_{PP}$ = 38 Hz).UV-Vis (CH₂Cl₂) λ_{max} [nm] (ϵ x 10⁻³, M⁻¹ cm⁻¹) 333 (3.61), 458 (0.230) CV (CH₂Cl₂, 100 mV) $E_{ap} = 0.053$ V Anal. Calcd. for C₃₅H₃₈Cl₂N₂OP₂Ru•0.5H₂O: C, 56.38; H, 5.27; N, 3.76. Found: C, 56.20 H, 5.18; N, 3.91.

trans-RuCl₂[Ph₂P(CH₂)₄PPh₂](ampy) (6). The complex was synthesized by the previously published method. The characterization data was in agreement with previously published data.¹⁰ UV-Vis (CH₂Cl₂) l_{max} [nm] (ϵ x 10⁻³) 384 (2.87), 458 (sh, 0.230). CV (CH₂Cl₂, 100 mV) E_{ap} = 0.112 V.

General Procedure for NMR Isomerization Reactions. Dissolved *trans*-RuCl₂(dppb)(ampy) (0.041 g, 0.057 mmol) was dissolved in 2 mL of CD₂Cl₂. The solution (600 μ L, 0.017 mmol) was added to a screwtop NMR tube and an internal capillary (0.0042 mmol of 1,3,5-trimethoxybenzene) was added to the tube. The NMR tube was heated at 308 K in an oil bath under light in the hood. A ¹H NMR spectrum (d1 = 15 s) was taken at room temperature every 75 minutes. The *ortho*-H on the pyridine (*trans*: 8.82 ppm and *cis*: 9.16 ppm) was integrated versus the aromatic hydrogens on 1,3,5-trimethoxybenzene (6.05 ppm).

General Procedure for UV-Vis Isomerization Reaction. In the glovebox a 0.25 mM solution of trans-RuCl₂(dppb)(ampy-L) (L = Cl, OMe and H) in CH₂Cl₂ was added to an air-free UV-Vis cuvette. During preparing and transformation of the solution, aluminum foil was used to avoid light exposure. The UV-Vis cuvette was heated to 308 K on a Unisoku cryostat in the presence of direct shining of white LED light, and the spectra were collected every 10 minutes.

General Procedure for Catalytic Transfer Hydrogenation in 2-propanol. Under air free conditions, the catalyst solution is prepared by adding the ruthenium complex (20 µmol) to 12 mL of 2-propanol with stirring. A second 0.1 M solution of NaOH in 2-propanol was prepared. The respected ketone (9.5 mL of a 0.1 M 2-propanol solution) was added to a flask and refluxed. The catalyst solution was generated by adding 1 mL of the NaOH solution to 1.5 mL of the Ru-solution. To each reaction flask containing ketone, 0.5 mL of the final Ru-NaOH solution was added and refluxed for the respective time. Following the reaction, the flasks were promptly placed into ice baths. The solution was then concentrated down on the rotovap. The final yield was determined by ¹H NMR spectroscopy with mesitylene as an internal standard.

Computational Methods. All calculations were performed using the Gaussian 16 package.⁴³ Geometry optimizations were performed in the gas phase using the M06 functional⁴⁴ with LANL2TZ(f) (Ru)⁴⁵ and 6-31+G(d)⁴⁶⁻⁵⁰ (Cl, P, N, C, H, O) basis sets (BS1). Frequency calculations at the same level of theory in each case were performed to validate stationary points, with zero imaginary frequencies reflecting ground state minima. Single-point self-consistent reaction field calculations (SCRF) were also performed using a larger basis set combination, LANL2TZ(f) (Ru) and 6-311++G(3df,2p) (Cl, P, N, C, H, O) (BS2), with the Polarizable Continuum Model (PCM)⁵¹ in dichloromethane. Redox potentials relative to Fc⁰/Fc⁺ were calculated by optimizing respective Ru^{II/III} and Fc⁰/Fc⁺ complexes followed by frequency calculation to obtain their respective thermochemical correction to Gibbs free energy and solvation calculation to obtain the solvation corrected total energy. TD-DFT calculations were performed by first optimizing complexes 1-6 in the gas phase with the PBE0 functional⁵² and BS1, followed by calculation of at least 10 singlet state excitations using PBE0 with BS2 and PCM (dichloromethane). Gabedit⁵³ was used to generate molecular orbital plots as well as computational UV-Vis spectra. JMol⁵⁴ was used to render images of optimized molecular structures.

ASSOCIATED CONTENT

Supporting Information

Full complex characterization including crystallographic data for complexes 1 and 2 (CCDC 2051101 and CCDC 2051102) (CIF), NMR spectra, UV-Vis spectra kinetics data, and computational results. This material is available free of charge via the Internet at

http://pubs.acs.org.

AUTHOR INFORMATION

Corresponding Author

* eejoslin@sewanee.edu

Funding. E.E.J: This work was supported by the American Chemical Society Petroleum Research

Fund [58300-UNI3] and The University of the South. I.G.-B. would like to thank the Robert A.

Welch Foundation (grant N-1900-20190330), the National Institutes of Health (NIH awards

R15GM128078 and R35GM137914) and the National Science Foundation (NSF CAREER

1941220) for financial support. G.M.F would like to thank NSF-CHE (grant #1039689) for

funding the X-ray diffractometer. N.N.B and B.V.P are grateful to the National Science

Foundation for support of computational work through an NSF Career Award (CHE-1752986).

The high-performance computing system (Thorny Flat) used in this research was supported by the

NSF Major Research Instrumentation (MRI) program (OAC-1726534).

Notes

The authors declare no competing financial interests.

Acknowledgements. The authors would like to thank Dr. Robert E. Bachman, The University of

the South and Dr. M. Zeller, Purdue University, for help solving the crystallographic data.

32

REFERENCES

- (1) Zafar, M.; Ramalakshmi, R.; Pathak, K.; Ahmad, A.; Roisnel, T.; Ghosh, S. Five-Membered Ruthenacycles: Ligand-Assisted Alkyne Insertion into 1,3-N,S-Chelated Ruthenium Borate Species. *Chem. Eur. J.* **2019**, *25* (59), 13537–13546. https://doi.org/10.1002/chem.201902663.
- (2) Gunanathan, C.; Milstein, D. Bond Activation and Catalysis by Ruthenium Pincer Complexes. *Chem. Rev.* **2014**, *114* (24), 12024–12087. https://doi.org/10.1021/cr5002782.
- (3) Pashaei, B.; Shahroosvand, H.; Graetzel, M.; Nazeeruddin, M. K. Influence of Ancillary Ligands in Dye-Sensitized Solar Cells. *Chem. Rev.* **2016**, *116* (16), 9485–9564. https://doi.org/10.1021/acs.chemrev.5b00621.
- (4) Joslin, E. E.; McMullin, C. L.; Gunnoe, T. B.; Cundari, T. R.; Sabat, M.; Myers, W. H. Coordination Chemistry of 4-Methyl-2,6,7-Trioxa-1-Phosphabicyclo[2,2,1]Heptane: Preparation and Characterization of Ru(II) Complexes. *Inorg. Chem.* **2012**, *51* (8), 4791–4801. https://doi.org/10.1021/ic300109b.
- (5) Navarro, M.; Segarra, C.; Pfister, T.; Albrecht, M. Structural, Electronic, and Catalytic Modulation of Chelating Pyridylideneamide Ruthenium(II) Complexes. *Organometallics* **2020**, *39* (13), 2383–2391. https://doi.org/10.1021/acs.organomet.0c00205.
- (6) Balaji, S.; Mohamed Subarkhan, M. K.; Ramesh, R.; Wang, H.; Semeril, D. Synthesis and Structure of Arene Ru(II) N ^ O-Chelating Complexes: *In Vitro* Cytotoxicity and Cancer Cell Death Mechanism. *Organometallics* **2020**, *39* (8), 1366–1375. https://doi.org/10.1021/acs.organomet.0c00092.
- (7) Ando, T.; Kamigaito, M.; Sawamoto, M. Catalytic Activities of Ruthenium(II) Complexes in Transition-Metal-Mediated Living Radical Polymerization: Polymerization, Model Reaction, and Cyclic Voltammetry ¹. *Macromolecules* **2000**, *33* (16), 5825–5829. https://doi.org/10.1021/ma9921596.
- (8) Tolman, C. A. Steric Effects of Phosphorus Ligands in Organometallic Chemistry and Homogeneous Catalysis. *Chemical Reviews* **1977**, *77* (3), 313–348. https://doi.org/10.1021/cr60307a002.
- (9) Jover, J.; Cirera, J. Computational Assessment on the Tolman Cone Angles for P-Ligands. *Dalton Trans.* **2019**, *48* (40), 15036–15048. https://doi.org/10.1039/C9DT02876E.
- (10) Baratta, W.; Herdtweck, E.; Siega, K.; Toniutti, M.; Rigo, P. 2- (Aminomethyl)Pyridine—Phosphine Ruthenium(II) Complexes: Novel Highly Active Transfer Hydrogenation Catalysts. *Organometallics* **2005**, *24* (7), 1660–1669. https://doi.org/10.1021/om0491701.
- (11) Hey, D. A.; Sauer, M. J.; Fischer, P. J.; Esslinger, E. H. J.; Kühn, F. E.; Baratta, W. Acetate Acetylacetonate Ampy Ruthenium(II) Complexes as Efficient Catalysts for Ketone Transfer Hydrogenation. *ChemCatChem* **2020**, *12* (13), 3537–3544. https://doi.org/10.1002/cctc.202000542.
- (12) Queiroz, S. L.; Batista, A. A.; Oliva, G.; do Pi. Gambardella, M. T.; Santos, R. H. A.; MacFarlane, K. S.; Rettig, S. J.; James, B. R. The Reactivity of Five-Coordinate Ru(II) (1,4-Bis(Diphenylphosphino)Butane) Complexes with the N-Donor Ligands: Ammonia, Pyridine, 4-Substituted Pyridines, 2,2'-Bipyridine, Bis(o-Pyridyl)Amine, 1,10-Phenanthroline, 4,7-Diphenylphenanthroline and Ethylenediamine. *Inorganica Chimica Acta* 1998, 267 (2), 209–221. https://doi.org/10.1016/S0020-1693(97)05615-6.

- (13) Ngo, H. L.; Hu, A.; Lin, W. Catalytic Asymmetric Hydrogenation of Aromatic Ketones in Room Temperature Ionic Liquids. *Tetrahedron Letters* **2005**, *46* (4), 595–597. https://doi.org/10.1016/j.tetlet.2004.11.150.
- (14) Hu, A.; Liu, S.; Lin, W. Immobilization of Chiral Catalysts on Magnetite Nanoparticles for Highly Enantioselective Asymmetric Hydrogenation of Aromatic Ketones. *RSC Adv.* **2012**, 2 (6), 2576. https://doi.org/10.1039/c2ra01073a.
- (15) Fang, X.; Li, B.; Zheng, J.; Wang, X.; Zhu, H.; Yuan, Y. Ruthenium Complexes with *N*-Functionalized Secondary Amino Ligands: A New Class of Catalysts toward Efficient Hydrogenation of Esters. *Dalton Trans.* **2019**, *48* (7), 2290–2294. https://doi.org/10.1039/C8DT04957B.
- (16) Hu, A.; Ngo, H. L.; Lin, W. 4,4'-Disubstituted BINAPs for Highly Enantioselective Ru-Catalyzed Asymmetric Hydrogenation of Ketones. *Org. Lett.* **2004**, *6* (17), 2937–2940. https://doi.org/10.1021/ol048993j.
- (17) O, W. W. N.; Lough, A. J.; Morris, R. H. Factors Favoring Efficient Bifunctional Catalysis. Study of a Ruthenium(II) Hydrogenation Catalyst Containing an N-Heterocyclic Carbene with a Primary Amine Donor. *Organometallics* **2012**, *31* (6), 2137–2151. https://doi.org/10.1021/om300108p.
- (18) Constable, D. J. C.; Dunn, P. J.; Hayler, J. D.; Humphrey, G. R.; Leazer, Jr., J. L.; Linderman, R. J.; Lorenz, K.; Manley, J.; Pearlman, B. A.; Wells, A.; Zaks, A.; Zhang, T. Y. Key Green Chemistry Research Areas—a Perspective from Pharmaceutical Manufacturers. *Green Chem.* **2007**, *9* (5), 411–420. https://doi.org/10.1039/B703488C.
- (19) Pattabiraman, V. R.; Bode, J. W. Rethinking Amide Bond Synthesis. *Nature* **2011**, *480* (7378), 471–479. https://doi.org/10.1038/nature10702.
- (20) Dunetz, J. R.; Magano, J.; Weisenburger, G. A. Large-Scale Applications of Amide Coupling Reagents for the Synthesis of Pharmaceuticals. *Org. Process Res. Dev.* **2016**, *20* (2), 140–177. https://doi.org/10.1021/op500305s.
- (21) Gladiali, S.; Alberico, E. Asymmetric Transfer Hydrogenation: Chiral Ligands and Applications. *Chem. Soc. Rev.* **2006**, *35* (3), 226–236. https://doi.org/10.1039/B513396C.
- (22) Yoshimura, M.; Tanaka, S.; Kitamura, M. Recent Topics in Catalytic Asymmetric Hydrogenation of Ketones. *Tetrahedron Letters* **2014**, *55* (27), 3635–3640. https://doi.org/10.1016/j.tetlet.2014.04.129.
- (23) Wang, D.; Astruc, D. The Golden Age of Transfer Hydrogenation. *Chem. Rev.* **2015**, *115* (13), 6621–6686. https://doi.org/10.1021/acs.chemrev.5b00203.
- (24) Doucet, H.; Ohkuma, T.; Murata, K.; Yokozawa, T.; Kozawa, M.; Katayama, E.; England, A. F.; Ikariya, T.; Noyori, R. Trans-[RuCl2(Phosphane)2(1,2-Diamine)] and Chiral Trans-[RuCl2(Diphosphane)(1,2-Diamine)]: Shelf-Stable Precatalysts for the Rapid, Productive, and Stereoselective Hydrogenation of Ketones. *Angewandte Chemie International Edition* **1998**, *37* (12), 1703–1707. https://doi.org/10.1002/(SICI)1521-3773(19980703)37:12<1703::AID-ANIE1703>3.0.CO;2-I.
- (25) Fujii, A.; Hashiguchi, S.; Uematsu, N.; Ikariya, T.; Noyori, R. Ruthenium(II)-Catalyzed Asymmetric Transfer Hydrogenation of Ketones Using a Formic Acid—Triethylamine Mixture. *J. Am. Chem. Soc.* **1996**, *118* (10), 2521–2522. https://doi.org/10.1021/ja9541261.
- (26) Kitamura, M.; Tokunaga, M.; Noyori, R. Asymmetric Hydrogenation of .Beta.-Keto Phosphonates: A Practical Way to Fosfomycin. *J. Am. Chem. Soc.* **1995**, *117* (10), 2931–2932. https://doi.org/10.1021/ja00115a030.

- (27) Yamakawa, M.; Ito, H.; Noyori, R. The Metal–Ligand Bifunctional Catalysis: A Theoretical Study on the Ruthenium(II)-Catalyzed Hydrogen Transfer between Alcohols and Carbonyl Compounds. *J. Am. Chem. Soc.* **2000**, *122* (7), 1466–1478. https://doi.org/10.1021/ja991638h.
- (28) Raynaud, C.; Norbert-Agaisse, E.; James, B. R.; Eisenstein, O. ³¹ P Chemical Shifts in Ru(II) Phosphine Complexes. A Computational Study of the Influence of the Coordination Sphere. *Inorg. Chem.* **2020**, acs.inorgchem.0c02256. https://doi.org/10.1021/acs.inorgchem.0c02256.
- (29) Santiago, M. O.; Filho, C. L. D.; Moreira, I. de S.; Carlos, R. M.; Queiroz, S. L.; Batista, A. A. Photochemical Isomerization of Trans- to Cis-[RuCl2(Dppb)(4,4'-X2-2,2'-Bipy)] (X=-H, -NO2, -Me, -COOH, -SMe, -OSMe, -Cl, -OMe) Complexes. *Polyhedron* **2003**, *22* (24), 3205–3211. https://doi.org/10.1016/j.poly.2003.07.007.
- (30) Shukla, M.; Srivastava, N.; Saha, S.; Rao, T. R.; Sunkari, S. Synthesis, Structure, UV–Vis–IR Spectra, Magnetism and Theoretical Studies on CuII[(2-Aminomethyl)Pyridine](Thiocyanate)2 and Comparisons with an Analogous CuII Complex. *Polyhedron* **2011**, *30* (5), 754–763. https://doi.org/10.1016/j.poly.2010.12.036.
- (31) Steck, E. A.; Ewing, G. W.; Nachod, F. Absorption Spectra of Heterocyclic Compounds. II. Amino-Derivatives of Pyridine, Quinoline and Isoquinoline. *J. Am. Chem. Soc.* **1948**, *70* (10), 3397–3406. https://doi.org/10.1021/ja01190a053.
- (32) Yenikaya, C.; Sarı, M.; Bülbül, M.; İlkimen, H.; Çelik, H.; Büyükgüngör, O. Synthesis, Characterization and Antiglaucoma Activity of a Novel Proton Transfer Compound and a Mixed-Ligand Zn(II) Complex. *Bioorganic & Medicinal Chemistry* **2010**, *18* (2), 930–938. https://doi.org/10.1016/j.bmc.2009.11.031.
- (33) Noyori, R.; Ohkuma, T. Asymmetric Catalysis by Architectural and Functional Molecular Engineering: Practical Chemo- and Stereoselective Hydrogenation of Ketones. *Angew. Chem. Int. Ed.* **2001**, *40* (1), 40–73. https://doi.org/10.1002/1521-3773(20010105)40:1<40::AID-ANIE40>3.0.CO;2-5.
- (34) de Araujo, M. P.; de Figueiredo, A. T.; Bogado, A. L.; Von Poelhsitz, G.; Ellena, J.; Castellano, E. E.; Donnici, C. L.; Comasseto, J. V.; Batista, A. A. Ruthenium Phosphine/Diimine Complexes: Syntheses, Characterization, Reactivity with Carbon Monoxide, and Catalytic Hydrogenation of Ketones. *Organometallics* **2005**, *24* (25), 6159–6168. https://doi.org/10.1021/om050182b.
- (35) Abdur-Rashid, K.; Lough, A. J.; Morris, R. H. RuHCl(Diphosphine)(Diamine): Catalyst Precursors for the Stereoselective Hydrogenation of Ketones and Imines ¹. *Organometallics* **2001**, *20* (6), 1047–1049. https://doi.org/10.1021/om001054k.
- (36) Shaw, A. P.; Ryland, B. L.; Norton, J. R.; Buccella, D.; Moscatelli, A. Electron Exchange Involving a Sulfur-Stabilized Ruthenium Radical Cation. *Inorganic Chemistry* **2007**, *46* (14), 5805–5812. https://doi.org/10.1021/ic700580u.
- (37) Comba, P.; Hunoldt, S.; Morgen, M.; Pietzsch, J.; Stephan, H.; Wadepohl, H. Optimization of Pentadentate Bispidines as Bifunctional Chelators for ⁶⁴ Cu Positron Emission Tomography (PET). *Inorganic Chemistry* **2013**, *52* (14), 8131–8143. https://doi.org/10.1021/ic4008685.
- (38) Nova, A.; Balcells, D.; Schley, N. D.; Dobereiner, G. E.; Crabtree, R. H.; Eisenstein, O. An Experimental—Theoretical Study of the Factors That Affect the Switch between Ruthenium-Catalyzed Dehydrogenative Amide Formation versus Amine Alkylation. *Organometallics* **2010**, *29* (23), 6548–6558. https://doi.org/10.1021/om101015u.

- (39) Bruker, APEX3 V2016.9-0, Bruker AXS Inc., Madison, Wisconsin, USA, 2019.
- (40) Sheldrick, G. M. Crystal Structure Refinement with *SHELXL. Acta Crystallogr C Struct Chem* **2015**, 71 (1), 3–8. https://doi.org/10.1107/S2053229614024218.
- (41) Barbour, L. J. X-Seed A Software Tool for Supramolecular Crystallography. *Journal of Supramolecular Chemistry* **2001**, *I* (4–6), 189–191. https://doi.org/10.1016/S1472-7862(02)00030-8.
- (42) Barbour, L. J. *X-Seed 4*: Updates to a Program for Small-Molecule Supramolecular Crystallography. *J Appl Crystallogr* **2020**, *53* (4), 1141–1146. https://doi.org/10.1107/S1600576720007438.
- (43) Frisch, M. J.; Trucks, G. W.; Schlegel, H. B.; Scuseria, G. E.; Robb, M. A.; Cheeseman, J. R.; Scalmani, G.; Barone, V.; Petersson,; G. A.; Nakatsuji, H.; Li, X.; Caricato, M.; Marenich, A. V.; Bloino, J.; Janesko, B. G.; Gomperts, R.; Mennucci, B.; Hratchian, H. P.; Ortiz, J.; V.; Izmaylov, A. F.; Sonnenberg, J. L.; Williams-Young, D.; Ding, F.; Lipparini, F.; Egidi, F.; Goings, J.; Peng, B.; Petrone, A.; Henderson,; T.; Ranasinghe, D.; Zakrzewski, V. G.; Gao, J.; Rega, N.; Zheng, G.; Liang, W.; Hada, M.; Ehara, M.; Toyota, K.; Fukuda, R.; Hasegawa, J.; Ishida, M.; Nakajima, T.; Honda, Y.; Kitao, O.; Nakai, H.; Vreven, T.; Throssell, K.; Montgomery, J. A., Jr.; Peralta, J. E.; Ogliaro, F.; Bearpark, M. J.; Heyd, J. J.; Brothers, E. N.; Kudin, K. N.; Staroverov,; V. N.; Keith, T. A.; Kobayashi, R.; Normand, J.; Raghavachari, K.; Rendell, A. P.; Burant, J. C.; Iyengar, S. S.; Tomasi, J.; Cossi, M.; Millam, J. M.; Klene, M.; Adamo, C.; Cammi, R.; Ochterski, J. W.;; Martin, R. L.; Morokuma, K.; Farkas, O.; Foresman, J. B.; Fox, D. J. Gaussian 16, Revision B.01; Gaussian, Inc.: Wallingford CT, 2016.
- (44) Zhao, Y.; Truhlar, D. G. The M06 Suite of Density Functionals for Main Group Thermochemistry, Thermochemical Kinetics, Noncovalent Interactions, Excited States, and Transition Elements: Two New Functionals and Systematic Testing of Four M06-Class Functionals and 12 Other Functionals. *Theor Chem Account* **2008**, *120* (1–3), 215–241. https://doi.org/10.1007/s00214-007-0310-x.
- (45) Roy, L. E.; Hay, P. J.; Martin, R. L. Revised Basis Sets for the LANL Effective Core Potentials. *J. Chem. Theory Comput.* **2008**, *4* (7), 1029–1031. https://doi.org/10.1021/ct8000409.
- (46) McLean, A. D.; Chandler, G. S. Contracted Gaussian Basis Sets for Molecular Calculations. I. Second Row Atoms, *Z* =11–18. *The Journal of Chemical Physics* **1980**, *72* (10), 5639–5648. https://doi.org/10.1063/1.438980.
- (47) Krishnan, R.; Binkley, J. S.; Seeger, R.; Pople, J. A. Self-consistent Molecular Orbital Methods. XX. A Basis Set for Correlated Wave Functions. *The Journal of Chemical Physics* **1980**, 72 (1), 650–654. https://doi.org/10.1063/1.438955.
- (48) Wachters, A. J. H. Gaussian Basis Set for Molecular Wavefunctions Containing Third-Row Atoms. *The Journal of Chemical Physics* **1970**, *52* (3), 1033–1036. https://doi.org/10.1063/1.1673095.
- (49) Hay, P. J. Gaussian Basis Sets for Molecular Calculations. The Representation of 3 *d* Orbitals in Transition-metal Atoms. *The Journal of Chemical Physics* **1977**, *66* (10), 4377–4384. https://doi.org/10.1063/1.433731.
- (50) Raghavachari, K.; Trucks, G. W. Highly Correlated Systems. Excitation Energies of First Row Transition Metals Sc–Cu. *The Journal of Chemical Physics* **1989**, *91* (2), 1062–1065. https://doi.org/10.1063/1.457230.

- (51) Scalmani, G.; Frisch, M. J. Continuous Surface Charge Polarizable Continuum Models of Solvation. I. General Formalism. *The Journal of Chemical Physics* **2010**, *132* (11), 114110. https://doi.org/10.1063/1.3359469.
- (52) Adamo, C.; Barone, V. Toward Reliable Density Functional Methods without Adjustable Parameters: The PBE0 Model. *The Journal of Chemical Physics* **1999**, *110* (13), 6158–6170. https://doi.org/10.1063/1.478522.
- (53) Allouche, A.-R. Gabedit-A Graphical User Interface for Computational Chemistry Softwares. *J. Comput. Chem.* **2011**, *32* (1), 174–182. https://doi.org/10.1002/jcc.21600.
- (54) Jmol: An Open-Source Java Viewer for Chemical Structures in 3D.